Non linear damping of a plate using Faraday instability of a fluid film

Jean-Michel Génevaux, Nicolas Dauchez, Olivier Doutres

Non linear damping of a plate using Faraday instability of a fluid film

J.M. Génevaux, N. Dauchez, O. Doutres

Laboratoire d'Acoustique de l'Université du Maine, Avenue Olivier Messiaen, 72085 LE MANS Cedex 9

Abstract

Damping using an instability of a fluid film in contact with a vibrating structure is investigated. Waves induced in the fluid film are the source of the added damping. A model based on the theory of Faraday instability is applied to a clamped circular plate covered by a fluid film. It is shown that this original technique can provide a significant damping, as with viscoelastic or porous material treatments. It is related to the amplitude of the waves which is a non linear function of the plate acceleration. Theoretical and experimental results are compared. The model overestimates the added damping: it is four times greater than the measured one.

Key words: Non linear damping, Damping of panels, Faraday instability, Fluid film, Vibroacoustics
PACS: 43.55.Wk, 46.40.Ff, 68.35.J, 43.25

1 Introduction

This paper examines a method to reduce the vibration and therefore the emitted noise of a structure by means of a fluid film in the low frequency range. The usual techniques for noise and vibration reduction from a structure use a viscoelastic layer bonded onto the structure [1]. In this case, the dissipation is proportional to the loss factor of the material and to the flexural strain energy of the viscoelastic layer. To be efficient, this technique requires the use of a thick layer. Its thickness, and therefore the mass adding, can be reduced by using a light and stiff constraining sheet that increases the strain energy in the dissipating layer. Optimal partial covering may also be used to reduce the added mass [2]. These techniques are limited by viscoelastic properties that depend on frequency and temperature [3]. Designed primarily for sound absorbing, porous materials such as polymer foam may also add significant damping when mounted onto a structure [4–6]. To improve the efficiency of

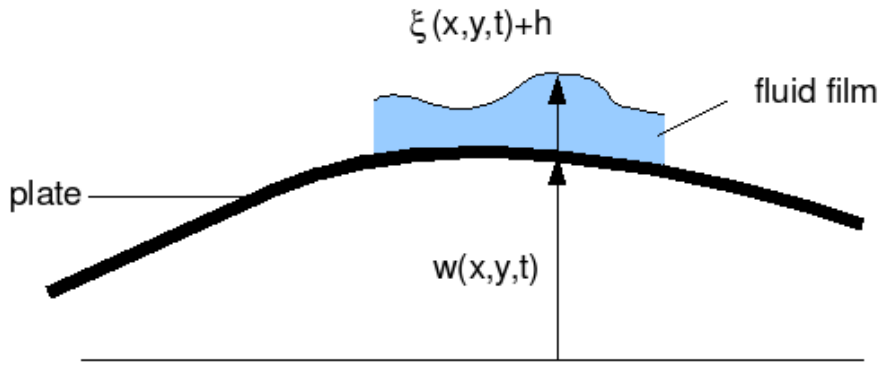

Fig. 1. Oscillation of a fluid film on a vibrating plate, with $w(x, y, t)$ the transverse displacement of a point P of the plate (coordinates in the plane (x, y)), t the time, h the water level of the fluid film at rest and $\xi(x, y, t)$ the amplitude of the waves above the point P.

passive treatments, active control techniques have also been developed [7, 8] but require more sophisticated set up. Moreover, their robustness has to be carefully demonstrated.

In this paper, damping added by a fluid film in contact with a structure is investigated (Fig. 1). When the normal acceleration of the structure is strong enough, stationary waves appear in the fluid film (Fig. 2). This phenomenon is called Faraday instability [9, 10]. In case of a finite area of the fluid-air interface, the boundary conditions select countable wave lengths and several stationary mode shapes are solution of the problem [11]. The mode shape which has the greater amplification coefficient appears [12, 13]. In case of an infinite area, this amplification coefficient will select the shape of the free surface among elementary cell patterns (roll, hexagon or square) (Fig. 2). These elementary cells can be considered as oscillators distributed over the surface of the structure [14], which damping depends on fluid flow in a cell and on the viscosity of the fluid. Moreover, the relation between the wave amplitude and the driving acceleration of the plate is nonlinear: it is necessary to determine the acceleration threshold for waves to appear and their amplitude at saturation [11, 15]. Note that for high acceleration level, ejection of droplets can be observed [16]. This paper focuses on the added dissipation to the structure by the Faraday instability, using the thinnest fluid layer without droplet ejections. To the author's knowledge, this technique aimed at reducing the vibration using the Faraday instability has not been previously presented.

In a first part (Sec. 2), the modelling the method of calculating the added damping is detailed. To this end, a particular geometrical configuration is chosen: a circular plate clamped at its edge.

In section 3, the corresponding experiment is designed in order to measure the added damping of the first mode of the plate. This highlights the nonlinear

Fig. 2. Stationary waves at the fluid-air interface (top view of the plate). Driving acceleration $W_a(0,0)$: 13.8 m s^{-2}

behaviour of the instability of the fluid film and the influence of the parameters governing the phenomenon.

The results of the model are compared with those obtained by the experiment in section 4.

2 Model

2.1 From local to global dissipation

This section details how to calculate the global dissipation added on the structure as function of the driving acceleration and for a given mode shape of the plate. Indeed, the modal dissipation is function of the area where the instabil-

ity appears and of the nonlinear relation between the amplitude of the waves and the local acceleration.

In the present paper, the first mode of a circular clamped plate of diameter d is considered. Its mode shape is given by [17],

$$\phi(r,\theta) = \frac{I_0(\beta_{01}d/2)\, J_0(\beta_{01}r) - J_0(\beta_{01}d/2)\, I_0(\beta_{01}r)}{I_0(\beta_{01}d/2)\, J_0(0) - J_0(\beta_{01}d/2)\, I_0(0)}, \tag{1}$$

with r the distance of the point to the centre of the plate, I_0 as the modified Bessel function, J_0 the Bessel function and $\beta_{01} = 1.015\frac{2\pi}{d}$. This mode shape is normalized so that $\phi(0,0) = 1$.

The modal damping ratio of the plate is given as function of modal parameters,

$$\zeta_{ap} = \frac{c_{ap}}{2\sqrt{k_p m_{pf}}}, \tag{2}$$

where c_{ap} is the damping coefficient added on the plate, k_p the modal stiffness of the plate and m_{pf} the modal mass of the plate loaded by the fluid film. These three terms c_{ap}, k_p and m_{pf} are calculated in the two following sections.

2.1.1 Modal stiffness and modal mass

The strain energy of the plate is calculated by integrating the local strain energy over the plate. This expression gives the modal stiffness k_p [17]:

$$\frac{1}{2}k_p\left(\phi(0,0)\right)^2 = \frac{1}{2}D\int_{\theta=0}^{2\pi}\int_{r=0}^{R}\left(\left(\phi_{,rr} + \frac{1}{r}\phi_{,r}\right)^2 - 2(1-\nu_p)\frac{\phi_{,rr}\phi_{,r}}{r}\right) r dr d\theta, \tag{3}$$

with D the stiffness of the plate defined by

$$D = Ee^3/(2(1-\nu_p^2)), \tag{4}$$

with E the Young modulus and ν_p the Poisson's ratio of the material, e the thickness of the plate. This modal stiffness does not depend on the fluid film properties.

By the same approach, the modal mass of the plate m_p is given by [17]:

$$\frac{1}{2}m_p\left(\phi(0,0)\right)^2 = \frac{1}{2}\int_{\theta=0}^{2\pi}\int_{r=0}^{R}\rho_p e\phi(r,\theta)^2 r dr d\theta, \tag{5}$$

with,

$$\rho_p e = \rho_s e + \rho_f h = \rho_s e(1+\tilde{\rho}), \tag{6}$$

the equivalent mass per unit area of the system, based on ρ_s the density of the aluminum, ρ_f the density of the fluid and an added mass due to the fluid

layer. In this equation, the kinetic energy of the fluid due to the flow relative to the plate is neglected. Assuming that ρ_p is constant along the plate and that $\phi(0,0) = 1$, equation (5) can be rewritten,

$$m_p = \rho_p e \int_{\theta=0}^{2\pi} \int_{r=0}^{R} \phi(r,\theta)^2 r dr d\theta. \tag{7}$$

The value of ρ_s is given by fitting the first resonance frequency of the bare plate,

$$f_1 = \frac{1.015^2}{2\pi} \frac{\pi^2}{(d/2)^2} \sqrt{\frac{D}{\rho_s e}}. \tag{8}$$

2.1.2 Added damping coefficient

The added damping coefficient c_{ap} is determined considering the dissipated energy during one period of the plate vibration [9, 12, 18–20],

$$\int_{t=0}^{2\pi/\omega_e} \frac{1}{2} c_{ap} \dot{w}^2(0,0,t) dt = \int_{t=0}^{2\pi/\omega_e} \left[\frac{1}{2} \int_{\theta=0}^{2\pi} \int_{r=0}^{R} \hat{c} \left(\frac{\partial h \alpha(r,\theta) \cos(\omega_f t)}{\partial t} \right)^2 r dr d\theta \right] dt, \tag{9}$$

with $w(0,0,t) = W \sin(\omega_e t)$ the instantaneous transverse displacement of the centre of the plate, W the amplitude of the displacement at this point, $\hat{c}$ the local damping coefficient per unit area, $\alpha(r,\theta) = A(r,\theta)/h$ (Eq. 12) the dimensionless amplitude of the waves , $A(r,\theta) = \max_t(\xi(r,\theta,t)$ the amplitude of the waves at saturation (Fig. 2), $\xi(r,\theta,t)$ the instantaneous position of the free surface, ω_f the circular frequency of the free surface waves due to the Faraday instability, ω_e the circular frequency of excitation and t the time.

Taking into account the axisymmetry of the first mode shape, that $\omega_f = \omega_e/2$ and $\dot{w}(0,0,t) = W\omega_e \sin(\omega_e t)$, the integration in time and in angle θ gives,

$$c_{ap} W^2 = \hat{c} h^2 \pi \int_{r=0}^{R} \alpha(r)^2 r dr. \tag{10}$$

The integration is made on the area where the instability appears. It is a disk of radius r_d, so that for $r > r_d$, $\alpha(r) = 0$. Assuming that the amplitude of the waves does not depend on the acceleration of the other points of the plate (local hypothesis), r_d may be defined by

$$\ddot{w}(r_d,\theta) = \tilde{\epsilon}_c g, \tag{11}$$

with $\tilde{\epsilon}_c$ the dimensionless acceleration threshold for the Faraday instability to appear and g the gravity.

For $r < r_d$, a linear relation between α^2 and $\tilde{\epsilon}$ is accounted for as suggested in ref. [11]: the amplitude of the waves at saturation, when $\frac{\partial A}{\partial t} = 0$, is an affine

function of $\tilde{\epsilon}$,

$$\alpha^2 = \tilde{\epsilon} A_{\omega_f} - B_{\omega_f}, \tag{12}$$

where A_{ω_f} and B_{ω_f} are two parameters which will be determined experimentally in this paper (Sec. 3 and Fig. 7). Note that $\tilde{\epsilon}_c$ is $\tilde{\epsilon}$ for $\alpha = 0$ in equation (12):

$$\tilde{\epsilon}_c = \frac{B_{\omega_f}}{A_{\omega_f}}. \tag{13}$$

Equation (10) then writes

$$c_{ap} = \frac{\pi \hat{c} h^2}{W^2} \left[A_{\omega_f} g \int_{r=0}^{r_d} \tilde{\epsilon}(r) r dr - B_{\omega_f} \int_{r=0}^{r_d} r dr \right], \tag{14}$$

where the dimensionless acceleration $\tilde{\epsilon}(r)$ can be related to $\phi(r, \theta)$ the normalized mode shape of the plate (Eq. 1) by

$$\tilde{\epsilon}(r) = \frac{W \omega_e^2}{g} \phi(r, \theta). \tag{15}$$

2.2 Equivalent damping coefficient of a fluid cell

The aim of this section is to calculate the modal damping coefficient $\hat{c}$ of the fluid per unit area, which is required to calculate c_{ap} (Eq. 14). It is given by,

$$\hat{c}(r, \theta) = 2 \zeta_0 m_f \omega_f, \tag{16}$$

with m_f the modal mass per unit area and ζ_0 the damping ratio of the fluid. ζ_0 can be related to the logarithmic decrement α_s of free oscillations [17] by

$$\zeta_0 = \frac{\alpha_s}{\sqrt{4\pi^2 + \alpha_s^2}}, \tag{17}$$

with $\alpha_s = 2\pi\delta k$ [15]. Here $\delta = \sqrt{2\nu/\omega_f}$ is the thickness of the viscous layer for a fluid with a kinematic viscosity ν solicited at the circular frequency ω_f, and k the wave number. This wave number is solution of [21]

$$\omega_f^2 = gk \tanh(kh) \left(1 + \frac{\sigma k^2}{\rho_f g} \right), \tag{18}$$

with σ the surface tension of the fluid-air interface.

The modal mass per unit area m_f is

$$m_f = \frac{m_{fcell}}{(\lambda/2)^2}, \tag{19}$$

with m_{fcell} the modal mass of one cell whose area is $(\lambda/2)^2$, with $\lambda = 2\pi/k$ the wave length. Here, the first mode of a fluid cell for a given pattern of the free surface is considered. Several patterns appear successively on the free surface with the increase of the level of the acceleration [10]: roll, hexagon, then square. In this paper, the square pattern which is present for high accelerations is chosen (Fig. 2). The modal shape can be defined according to a potential function for the flow: the Reynolds is large enough ($Re = 1.7\ 10^6$) for the thickness of viscous boundary layer ($\delta = 0.063$ mm) to be smaller than the fluid depth. Let us consider a fluid cell defined by a volume of incompressible fluid whose dimensions are $\lambda/2$ in $\mathbf{x}$ and $\mathbf{y}$ directions, and h in $\mathbf{z}$ direction. Symmetry arguments allow the use of a flow $\mathbf{v}$ relative to the plate associated to $\Phi_f(x, y, z, t) = \phi_f(x, y, z)g(t)$, with $g(t)$ a harmonic function and

$$\phi_f(x, y, z) = \beta(r, \theta)\cos(q(2x/\lambda - 1))\cos(q(2y/\lambda - 1))\cosh(\sqrt{2}q, z/\lambda), \quad (20)$$

with β the amplitude of the potential function which depends on the position of the fluid cell (cylindrical coordinates r,θ), and (x,y,z) the coordinates of a point into the cell. The velocity field $\mathbf{v}$ is given by,

$$h\frac{\partial\phi_f}{\partial x}g(t) = \mathbf{v}.\mathbf{x},\ h\frac{\partial\phi_f}{\partial y}g(t) = \mathbf{v}.\mathbf{y},\ h\frac{\partial\phi_f}{\partial z}g(t) = \mathbf{v}.\mathbf{z}. \quad (21)$$

The boundary conditions at $x = \lambda/2$ and $y = \lambda/2$ give for the first mode of the fluid cell, $q = \pi$.

The kinetic energy of the fluid in the cell is used to calculate m_{fcell}:

$$\begin{aligned} &\tfrac{1}{2}m_{fcell}\left(\tfrac{\partial\alpha(r,\theta)\cos(\omega_f t)}{\partial t}\right)^2 = \\ &\qquad \tfrac{1}{2}\rho_f g(t)^2 \int_{x=0}^{\lambda}\int_{y=0}^{\lambda}\int_{z=0}^{h}\left(\phi_{f,x}^2 + \phi_{f,y}^2 + \phi_{f,z}^2\right)dxdydz, \end{aligned} \quad (22)$$

with $\phi_{f,x} = \frac{\partial f}{\partial x}$. $\beta(r, \theta)$ is derived from $\alpha(r, \theta)$ the amplitude of the waves, by equating the vertical velocity of a point of the free surface ($z = h$):

$$\alpha(r, \theta)\frac{\partial\cos(\omega_f t)}{\partial t} = g(t)\frac{\partial\phi_f}{\partial z} \quad \forall t, \quad (23)$$

and using equation (20) it gives,

$$\alpha(r, \theta) = \beta(r, \theta)\frac{2\sqrt{2}\pi}{\lambda}\sinh(\sqrt{2}\pi h/\lambda), \quad (24)$$

$$g(t) = -\omega_f \sin(\omega_f t) \quad (25)$$

so that,

$$\beta(r, \theta) = \frac{\alpha(r, \theta)\lambda}{2\sqrt{2}\pi\sinh(\sqrt{2}\pi h/\lambda)}. \quad (26)$$

Using equation (26), and integrating the second member of equation (22), the modal mass of the 1 degree of freedom system associated to the fluid cell writes,

$$m_{fcell} = \frac{\rho_f \lambda^3 \sqrt{2}}{256\pi} \frac{\left(1 - \exp\left(\frac{-8\sqrt{2}\pi h}{\lambda}\right)\right) \exp\left(\frac{4\sqrt{2}\pi h}{\lambda}\right)}{\cosh\left(\frac{\sqrt{2}\pi h}{\lambda}\right)^2 - 1}. \tag{27}$$

The modal mass per unit area m_f and the modal damping coefficient by unit area $\hat{c}$ may be obtained with equations (16) and (19).

3 Experimental results

The aim of this section is to determine experimentally the plate damping induced by the Faraday instability of the fluid film. Because the system is nonlinear, all experimental quantities are referenced to the acceleration at the centre of the plate, called driving acceleration, and denoted $W_a(0,0)$. Four water levels and four values of the driving acceleration are considered.

3.1 Experimental set-up

The geometrical configuration is presented in figure 3. A circular aluminum plate of diameter $d = 0.290$ m is clamped. Its characteristics are summarized in tables 1 and 2. It is excited by a shaker connected to its centre via a force transducer giving the excitation force F. An accelerometer of mass $m_a = 0.0042$ kg is bonded at 1 cm of the centre of the plate to get the reference acceleration $W_a(0,0) = \omega_e^2 W$. A laser vibrometer is focused on the plate through the fluid film. The laser spot area is less than gives a measured area of the order of 1 mm^2.

The frequency range is set between 40 Hz and 120 Hz to ensure Faraday instabilities for experimentally achievable accelerations. The thickness of the fluid layer is chosen to be of the order of the wavelength: this ensures a total covering of the plate and a small added mass.

The frequency response functions are obtained using a step by step harmonic excitation for a constant acceleration amplitude $W_a(0,0)$.

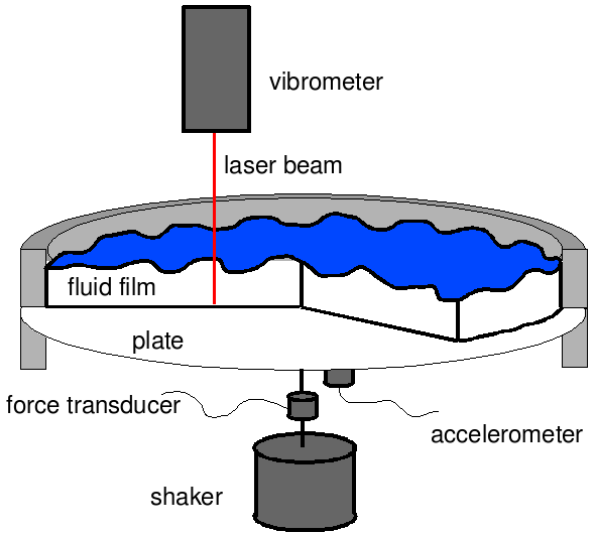

Fig. 3. Experimental set-up.

3.2 Determination of the free surface velocity of the fluid

The signal given by the laser vibrometer is proportional to the apparent velocity of the plate $\frac{d\tilde{w}}{dt}$. It is a combination of the plate and of the free surface velocities:

$$\frac{d\tilde{w}(r,\theta,t)}{dt} = \frac{dw(r,\theta,t)}{dt} - \left(\frac{c_0}{c_1} - 1\right) \frac{d(h+\xi(r,\theta,t))}{dt}, \tag{28}$$

with $w(r,\theta,t)$ the displacement of the plate at the point $P(r,\theta)$, c_0 the light velocity in the air, c_1 the light velocity in the fluid, $h(r,\theta,t)$ the water level crossed by the beam. The time signal of the apparent speed of the plate (Fig. 4) exhibits a sub-harmonic at $\omega_e/2$. Their contributions can be easily identified because they are at different frequencies (see Fig. 4). To do so, equation (28) is rewritten as:

$$\frac{d\tilde{w}(r,\theta,t)}{dt} = \tilde{a}_1 \cos(\omega_e t + \tilde{a}_2) + \tilde{a}_3 \cos\left(\frac{\omega_e}{2} t + \tilde{a}_4\right). \tag{29}$$

The parameters $\tilde{a}_1$ and $\tilde{a}_2$ are associated to the plate velocity, and the parameters $\tilde{a}_3$ and $\tilde{a}_4$ to the fluid interface movement. They are determined using a nonlinear optimization. The position of the nodes of the free surface mode shape are not stationary: $\tilde{a}_3 = 0$ if the laser beam focuses through a node, and is maximum if the laser beam focuses through an antinode. Indeed, for level of accelerations far higher the threshold, second order effects [22] induce a slow drift of the positions of the antinode of the fluid air interface. Thus, the time of acquisition must be long enough to contain measurement on an antinode. The amplitude of the waves is then deduced from the greatest value of $\tilde{a}_3$.

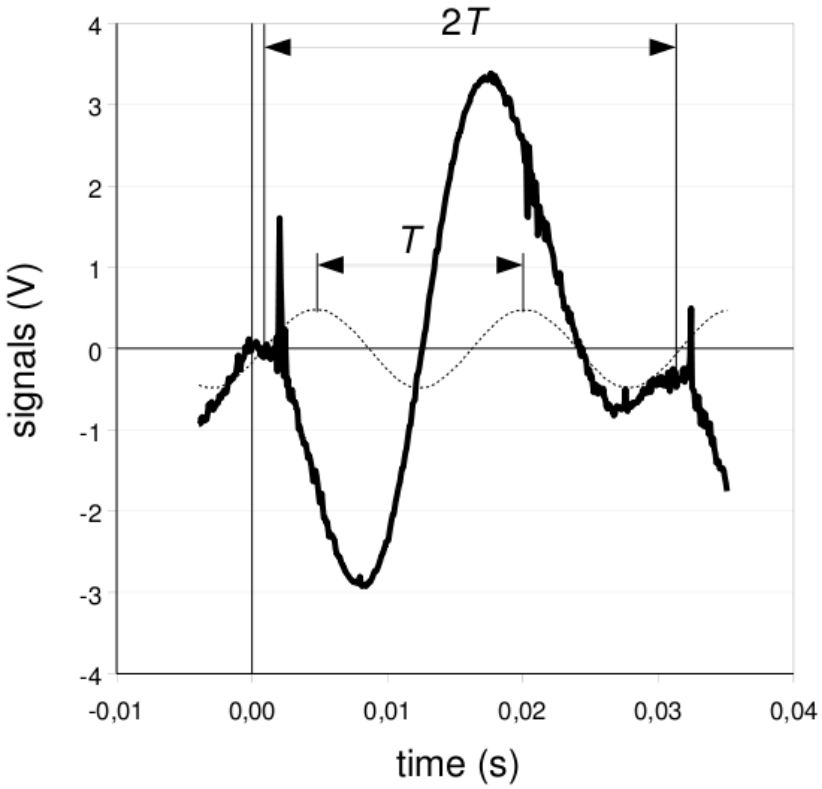

Fig. 4. Signals (V) of the acceleration of the plate (dotted line 31.6 m s^{-2}/ V) and its apparent velocity measured by the laser vibrometer (bold line 0.025 m s^{-1} / V) maximum velocity of the plate : 0.039 m s^{-1} ; water level 0.0046 m ; $\tilde{\rho} = 0.88$; frequency of excitation 65 Hz.

3.3 Influence of the driving acceleration and water levels

The experiments are performed with water to test the influence of the fluid level on the frequency response functions. The water levels remain below 0.0133 m and above 0.004 m for all the experiments. Below this lower limit, the wetting mechanism prevents the water from covering the whole plate. The ratio of added mass per unit area is:

$$\tilde{\rho} = \frac{\rho_f h}{\rho_s e}. \tag{30}$$

Near the resonance frequency (75 Hz), stationary waves are observed on the free surface (Fig. 2). Their amplitude is higher at the centre of the plate. This coincides with the maximum amplitude of the first mode shape. They appear as square patterns within a circle at the centre of the plate. Their wavelength, which are consistent with capillarity waves on the surface, increases as the frequency decreases.

To determine the acceleration threshold for Faraday instability, the frequency response function is measured for several amplitudes of the driving acceleration for water levels from 0 to 0.0133 m. Nonlinear effects are observed (Fig. 5) when increasing the amplitude of acceleration:

- the existence of a threshold for waves to appear,
- an increase in the area of the circular surface on which waves are present,
- a slight increase in the frequency resonance,
- a reduction of the amplitude of the peak (up to 13 dB).

In figure 5, the threshold is between 6 m s^{-2} and 13 m s^{-2}. It corresponds to a sharp increase in damping. Figure 6 shows damping ratio ζ_{pf} which is estimated using the half-power method. The measured damping for this non optimized configuration can be half the value of the damping measured in the case of unconstrained-layer treatment, and is greater than the damping added by foam or fiber layer. This increase is not observed for the bare plate (continuous line). The thinner the fluid layer, the stronger the damping is.

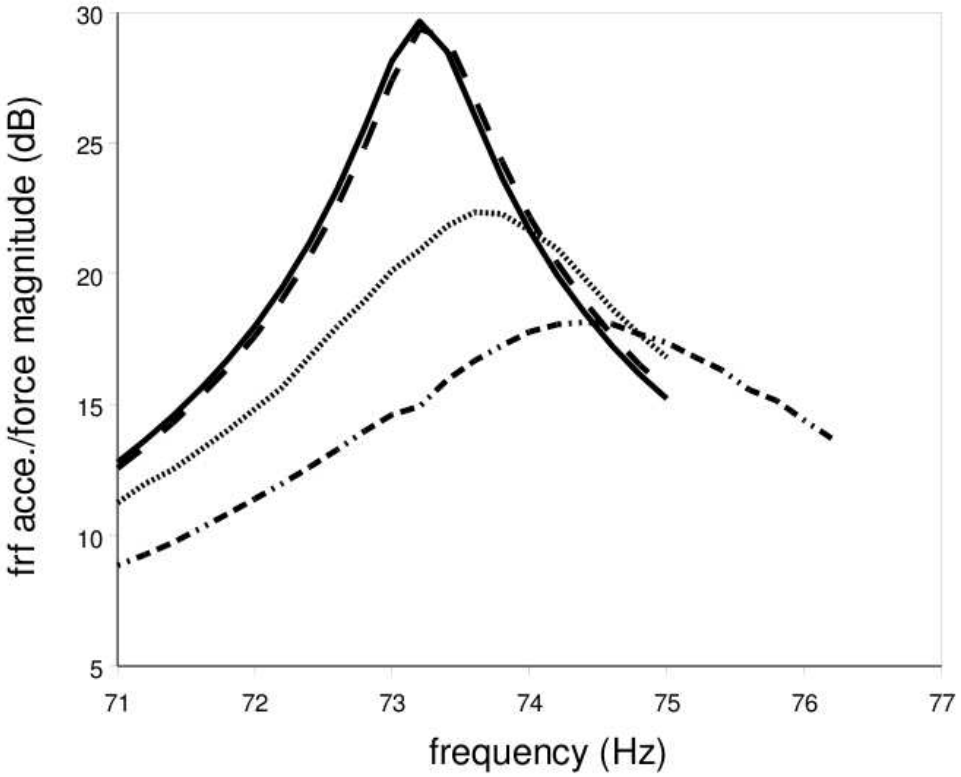

Fig. 5. Influence of the driving acceleration $W_a(0,0)$ on the frequency response function (accelerometer/force) for a water level of 0.0046 m, $\tilde{\rho} = 0.88$: continuous line, $W_a(0,0) = 3.16$ m s^{-2} ; dashed line, $W_a(0,0) = 6.32$ m s^{-2} ; dotted line, $W_a(0,0) = 12.7$ m s^{-2} ; dashed dotted line, $W_a(0,0) = 25.3$ m s^{-2}.

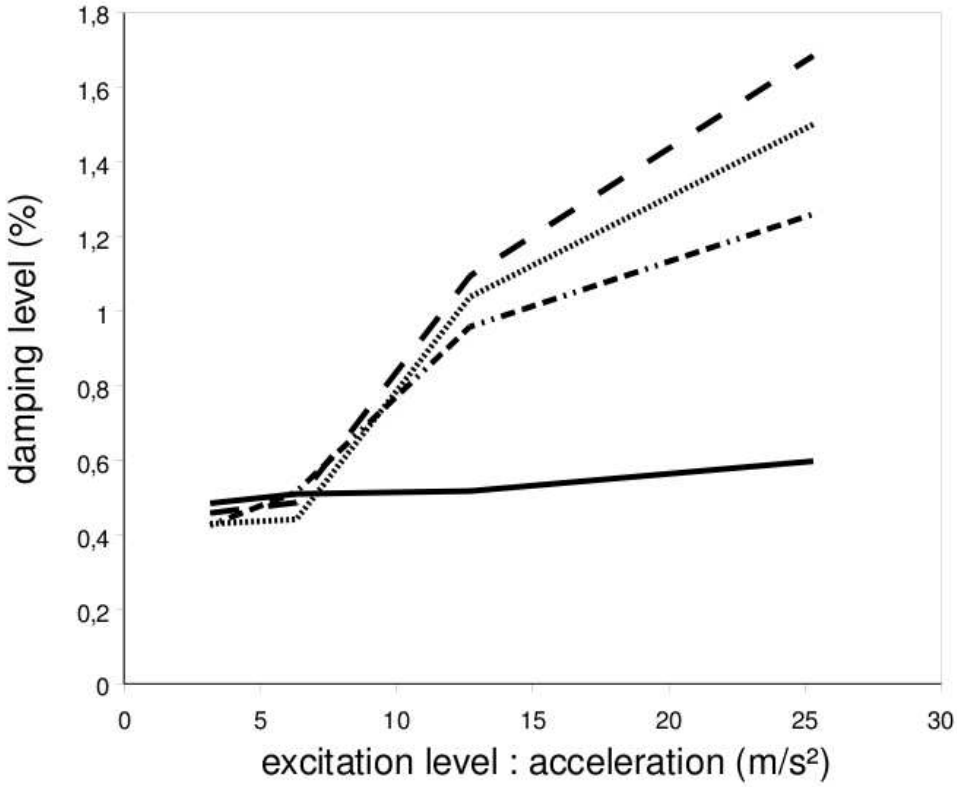

Fig. 6. Influence of the driving amplitude $W_a(0,0)$ on the plate damping for several water levels: continuous line, 0.0 m ; dashed line, 4.6 mm ; dotted line, 8.0 mm ; dashed dotted line, 13.3 mm.

4 Comparison between theoretical and experimental results

Comparison between theoretical and experimental values of the plate damping induced by the fluid film is now evaluated. Water with the thinner thickness is used to induce the stronger damping. The numerical values of the parameters of the model are given in tables 1 and 2 for this configuration.

The added damping ratio depends on the local dissipation of the fluid layer and on the area of the instability area.

This local dissipation is a function of the relation between the local acceleration of the plate and of the wave amplitude (Fig. 6). The relation between the wave amplitude and the motion of the plate is quantified by the coefficients A_{ω_f} and B_{ω_f} (Eq. (12)) which are identified on the experimental data by a least-squares regression method (Fig. 7). The uncertainties on the position of the regression line are calculated with a confidence of 95%. Note that three points are not taken into account: the noise on the signal and the low spatial stability of the waves do not allow a correct evaluation of the amplitude of the

Table 1
Numerical inputs of the model.

Plate		
Diameter of the plate (m)	d	0.290
Thickness of the plate (m)	e	0.001
Material of the plate		aluminum
Young's Modulus (Pa)	E	$7\,10^{10}$
Poisson's ratio	ν_p	0.3
Frequency of the first resonance of the bare plate (Hz)	f_1	100
Frequency of excitation (Hz)	f_e	75
Fluid		
Gravity (ms^{-2})	g	9.81
Fluid layer thickness (m)	h	0.0046
Kinematic viscosity of water (m^2s^{-1})	ν	10^{-6}
Density of the fluid (kg m^{-3})	ρ_f	1000
Wave length of the free surface (m)	λ	0.0063
First amplitude of the wave coefficient	A_{ω_f}	$[0.0135, 0.0163]$
Second amplitude of the wave coefficient	B_{ω_f}	$[0.0111, 0.0134]$

waves for these three acceleration levels. In the following, above the threshold $\tilde{\epsilon}_c$, the dimensionless amplitudes of the waves lie in the following boundaries:

$$0.0135(\tilde{\epsilon} - 0.82) < \alpha^2 < 0.0163(\tilde{\epsilon} - 0.82). \tag{31}$$

The wave length $\lambda = 0.004$ m given by the model using $\sigma = 0.072$ N m^{-1} the surface tension of the fluid-air interface, is near the measured experimental wave length (0.00626 m$< \lambda <$ 0.00634 m, Sec. 3.3). The experimental average value $\lambda = 0.0063$ m is used in the model to evaluate the damping.

Moreover, the equivalent damping coefficient c_{ap} added to the structure depends on the area on which the damping occurs. The first mode shape of the plate induces a circular limit of instability of radius r_d where, $W_a(r_d, \theta) = 8.04$ m s^{-2}. The relationship between this radius and the acceleration in the centre of the plate is given by the mode shape of the plate $\phi(r, \theta)$ (Eq. 1) and the instability threshold. The evolution of c_{ap}, as function of W_a at the centre of the plate, can then be calculated taking into account the uncertainty of the amplitude of the waves (Eq. 31). From the evolution of c_{ap}, the damping ratio added by the fluid ζ_{ap} can be plotted (Fig. 8).

Table 2
Numerical outputs of the model.

Loaded plate			
Stiffness of the plate (N m)	Eq. (4)	D	8.82
Dimensionless added mass	Eq. (30)	$\tilde{\rho}$	0.88
Density of the plate with air loading (kg m^{-3})	Eq. (8)	ρ_s	5230
Modal stiffness (Nm^{-1})	Eq. (3)	k_p	1.08 105
Equivalent mass of the plate with fluid (kgm^{-3})	Eq. (6)	ρ_p	7215
Modal mass (kg)	Eq. (7)	m_p	0.0875
Fluid			
Threshold of instablility (ms^{-2})	Eq. (13)	$\tilde{\epsilon_c} g$	8.04
Local damping ratio of the fluid	Eq. (17)	ζ_0	14.5%
Modal mass of a fluid cell (kg)	Eq. (27)	m_{fcell}	$2.23\,10^{-6}$
Modal mass per unit area (kg m^{-2})	Eq. (19)	m_f	$2.25\,10^{-1}$
Equivalent damping coefficient per unit area (kg $m^{-2}s^{-1}$)	Eq. (16)	$\hat{c}$	9.69
Damping ratio added by the fluid	Eq. (2)	ζ_{ap}	Fig. 6

For the experimental point of view, the damping ratio added by the fluid can be deduced by the comparison of the damping ratio observed with the fluid ζ_{pf} and the damping ratio of the bare plate ζ_p (Fig. 6). The damping ratio of the bare plate is,

$$\zeta_p = \frac{c_p}{2\sqrt{k_p m_p}}, \tag{32}$$

with c_p the modal damping coefficient of the plate, m_p the modal mass of the plate. With the fluid layer the damping ratio is given by,

$$\zeta_{pf} = \frac{c_p + c_{ap}}{2\sqrt{k_p m_{pf}}} = \frac{c_p}{2\sqrt{k_p m_{pf}}} + \zeta_{ap}. \tag{33}$$

By neglecting the kinetic energy of the waves compared to the kinetic energy of the loaded plate, the relation $m_{pf} = m_p(1 + \tilde{\rho})$ gives,

$$\zeta_{pf} = \frac{c_p}{2\sqrt{k_p m_p(1 + \tilde{\rho})}} + \zeta_{ap}. \tag{34}$$

Thus, the experimental value of the added damping ratio is

$$\zeta_{ap} = \zeta_{pf} - \zeta_p \frac{1}{\sqrt{1 + \tilde{\rho}}}. \tag{35}$$

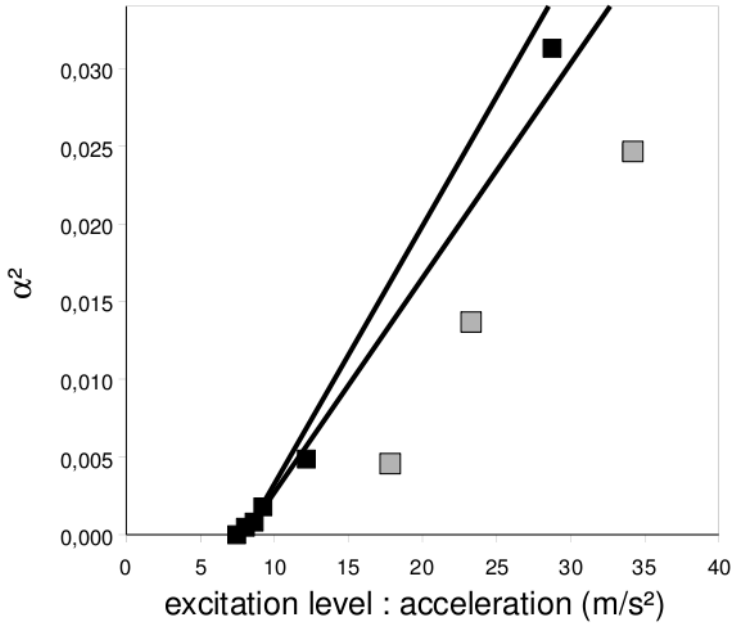

Fig. 7. Experimental evolution of the dimensionless oscillation amplitude $\alpha = A/h$ with the acceleration above the threshold for a given frequency (75 Hz) with water. The two lines corresponds to the uncertainty with a confidence of 95% of the mean square line which fits the data.

The comparison (Fig. 8) between experimental and theoretical values of ζ_{ap} shows that above the threshold the amplitude of the theoretical damping is four times greater than the experimental damping.

The source of this discrepancy can be sought in the high sensitivity of the model to the amplitudes of the waves. The relation between the wave amplitude and the acceleration has been determined assuming a locally reacting behaviour of each fluid cell. This hypothesis is valid where the acceleration is uniform: this is the case in the vicinity of an antinode (centre of the plate for the first mode). This assumption may not be valid where an acceleration gradient is present. Moreover, in this transition region, the cell shape is no longer square (Fig. 2).

Nevertheless, note that the damping added by the fluid film is comparable to thoses obtained with viscoelastic or porous material treatments [1, 6].

5 Conclusion

Damping of a vibrating structure by means of a heavy fluid film subjected to Faraday instability has been studied. It is shown that added damping may be

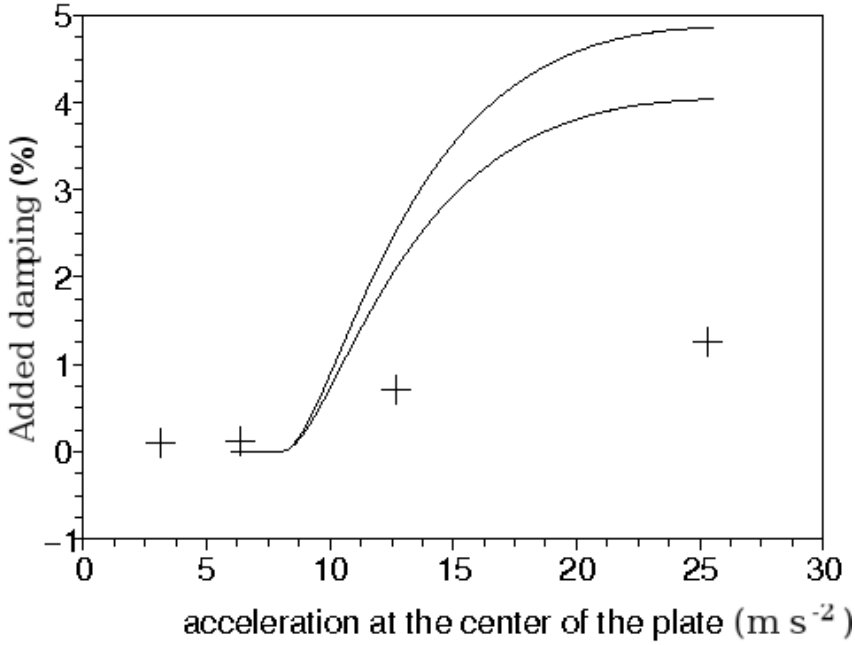

Fig. 8. Evolution of the damping ratio added by the fluid versus the driving acceleration $W_a(0,0)$: theoretical values (between the two lines: the uncertainties on the measurement of the water waves induce two curves of dimensionless damping with 95% of confidence), experimental values (crosses)

.

significant. A model has highlighted the governing parameters: the acceleration threshold and the amplitude of the waves, which depend on the frequency, on the viscosity and the fluid thickness of the fluid and on the mode shape of the structure. The model takes into account that the dissipation does not act on the overall structure. Experimental results have confirmed the tendencies of the predicted damping. Nevertheless, the model overestimates the added damping: it is four times greater than the measured one. Further experiments are needed to detect the sources of discrepancies: the Faraday instability threshold and the amplitude of the waves must be studied in the case of non uniform acceleration.

ACKNOWLEDGMENTS

Thanks to Lazhar Benyahia from the Laboratoire Polymères, Colloides, Interfaces of Université du Maine (Le Mans, France) for our productive discussions. Thanks to Denis Ritter for the English corrections.

References

[1] A.D. Nashif, D.I.G. Jones, J.P. Henderson, *Vibrations damping*, J. Wiley & sons, 1985

[2] M. Alvelid, *Optimal position and shape of applied damping material* Journal of Sound and Vibration **310** pp 947-965, 2008

[3] T. Pritz, *Loses factor peak of viscoelastic materials : magnitude to width relations* Journal of Sound and Vibration, **246**,2, pp265-280, 2001

[4] 0. Doutres, N. Dauchez, J.M. Génevaux, *Validity of the limp model for porous materials: A criterion based on Biot theory*, J of Acoustical Society of America **122**, pp2038-2048, 2007

[5] 0. Doutres, N. Dauchez, J.M. Génevaux, *Porous layer impedance applied to a moving wall : Application to the radiation of a covered piston*, J of Acoustical Society of America **121**,1, pp206-213, 2007

[6] N. Dauchez, S. Sahraoui, N. Atalla, *Investigation and modelling of damping in a plate with a bonded porous layer*, Journal of Sound and Vibration, **265**,2 , pp437-449, 2003

[7] A. Baz, *Robust control of active constrained layer damping*, Journal of Sound and Vibration, **211**, 3, pp467-480, 1998

[8] D. Guyomar, A. Badel, *Nonlinear semi-passive multimodal vibration damping: An efficient probabilistic approach* Journal of Sound and Vibration, **294**,1-2, pp249-268, 2006

[9] L. Faraday, *On the forms and states of fluids on vibrating elastic surfaces*, Philos. Trans. Royal Inst., London, **121**, p229, 1831

[10] A. V. Kityk, K. Knorr, H.-W. Muller and C. Wagner, *Spatio-temporal Fourier analysis, of Faraday surface wave patterns on a two-liquid interface*, Europhysics letter **65**,6, pp857-863, 2004

[11] S. Douady, *Experimental study of the Faraday instability*, J. of Fluid Mech., **221**, pp383-409, 1990

[12] T.B. Benjamin, F. Ursell, *The stability of the plane free surface of a liquid in vertical periodic motion* Proc Royal Soc. of London, A, **225**, pp505-515, 1934

[13] A. Merlen,Z. Qi,P. Voinovich,E. Timofeev, *Duality of the supercritical solutions in magnetoacoustic wave phase conjugation*, Wave Motion (to be published)

[14] D.J. Thompson, *A continuous damped vibration absorber to reduce broadband wave propagation in beams*, Journal of Sound and Vibration **311** pp824-842, 2008

[15] S.T. Milner, *Square patterns and secondary instabilities in driven capillary waves*, J. Fluid Mech., **225**, p81-100, 1991

[16] S. Alzuaga, J.-F. Manceau, F. Bastien *Motion of droplets on solid surface using acoustic radiation pressure* Journal of Sound and Vibration, **282**, pp151-162, 2005

[17] M. Geradin, D. Rixen, *Théorie des vibrations : application à la dynamique des structures* Masson, Paris, 1993

[18] L. Matthiessen, *Ueber die Transversalschwingungen tnender tropfbarer und elastischer Flssigkeiten* Annalen der Physik, **217**,11 , p375-393, 1870

[19] L. Rayleigh, *On the crispation of fluid resting upon a vibrating support.* Phil. Mag. **5**,5, pp50-58, 1883

[20] A.O. Maksimov, T.G. Leighton, *Transient processes near the threshold of acoustically driven bubble shape oscillations*, Acta Acustica, 87(3), 2001, 322-32

[21] J.M. Génevaux, X.J. Chai, J.P. Brancher, *Gravity effects on coupled frequencies of a 2D fluid-structure problem with free surface*, J. of Sound and Vibrations, **215**,2, pp331-342, 1998

[22] E. Martin, C. Martel, J.M. Vega, *Drift instability of standing Faraday waves* Journal of Fluid Mechanics **467**, pp57-79, 2002

List of Figures

List of Tables